NASA TECHNICAL MEMORANDUM

NASA TM X-71674

NASA TM X-71674

GENERALIZED WAVE ENVELOPE ANALYSIS OF SOUND PROPAGATION IN DUCTS WITH STEPPED NOISE SOURCE PROFILES AND VARIABLE AXIAL IMPEDANCE

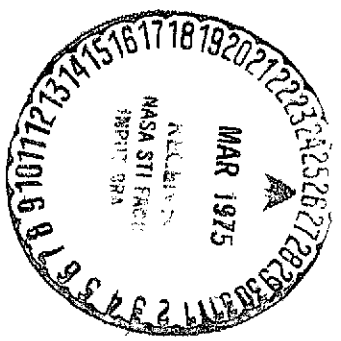

by Kenneth J. Baumeister
Lewis Research Center
Cleveland, Ohio 44135

TECHNICAL PAPER proposed for presentation at
Second Aeronautics Specialists Conference
sponsored by the American Institute of Aeronautics and Astronautics
Hampton, Virginia, March 24-26, 1975

GENERALIZED WAVE ENVELOPE ANALYSIS OF SOUND PROPAGATION IN DUCTS WITH STEPPED NOISE SOURCE PROFILES AND VARIABLE AXIAL IMPEDANCE

Kenneth J. Baumeister†
Lewis Research Center
National Aeronautics and Space Administration
Cleveland, Ohio

E-7941

Abstract

A finite difference formulation is presented for sound propagation in a rectangular two-dimensional duct without steady flow. Before the difference equations are formulated, the governing Helmholtz equation is first transformed to a form whose solution tends not to oscillate along the length of the duct. This transformation reduces the required number of grid points by an order of magnitude. Example solutions indicate that stepped noise source profiles have much higher attenuation than plane waves in a uniform impedance liner. Also, multiple stepped impedance liners are shown to have higher attenuation than uniform ducts if the impedances are chosen properly. For optimum noise reduction with axial variations in impedance, the numerical analysis indicates that for a plane wave input the resistance should be near zero at the entrance of a suppressor duct, while the reactance should be near the optimum value associated with the least-attenuated mode in a uniform duct. A close-packed array of quarter wave tubes tuned to the proper impedance may approximate this optimum condition in the entrance region of the liner. The low resistance entrance region of a segmented liner redistributes the acoustic energy nearer to the wall where it can be more effectively absorbed.

Introduction

In engine ducts which have variations in axial impedance, area, or flow, the finite difference approach is an attractive alternate to the conventional analytical techniques currently used in noise propagation analysis. In Refs. 1 to 3, the conventional finite difference theory has been applied to the problem of sound propagation in two-dimensional straight hard- and soft-wall ducts with and without steady flow. In Ref. 4, the difference technique was applied to the variable area case. In all the above, the continuous acoustic field is lumped into a series of grid points at which the acoustic pressure and velocity are determined (as in Fig. 1). For long ducts and high frequency sound propagation, large computer storage is required. To eliminate this storage requirement, a wave envelope concept was developed(5) which greatly reduced the number of grid points necessary to solve a problem. However, under certain conditions, the author indicated in Ref. 5 that the transformation was not appropriate or advantageous. This paper presents a generalization which removes the limitations of the earlier theory.

Herein, a finite difference technique is formulated for sound propagation in a rectangular two-dimensional duct without steady flow. First, the governing Helmholtz equation is transformed into a form which reduces the required number of grid points in the conventional finite difference theory by an order of magnitude. This technique is labeled the Generalized Wave Envelope Concept. Next, this concept is applied to a duct with variable axial impedance for a plane wave input. In addition, the effect of stepped noise source profiles on the attenuation of uniform impedance liners is investigated.

List of Symbols

A	coefficient matrix
c	velocity of sound
ΔdB	decrease in decibels
E	acoustic power
F	column vector
f	frequency
H	duct height
I	dimensionless intensity
i	$\sqrt{-1}$
L	dimensionless length of duct
m	total number of grid rows (points in y-direction)
n	total number of grid columns (points in x-direction)
P	dimensionless pressure, P(x,y), Eq. (1)
p	dimensionless pressure, p(x,y), Eq. (7)
$\bar{p}$	dimensionless column pressure vector
S	source strength
x	dimensionless axial coordinate
Δx	axial grid spacing
y	dimensionless transverse coordinate
Δy	transverse grid spacing
Z	impedance
ζ	dimensionless specific acoustic impedance
η	dimensionless frequency, Eq. (2)
η^+	wave envelope frequency
λ	pressure wavelength
λ^+	effective wavelength

Subscripts

i,j axial and transverse indexes, see Fig. 1

Superscripts

(1) real part

(2) imaginary part

Governing Equations

The governing equation describing the steady state propagation of sound is the classic Helmholtz equation (dimensionless form)

†Aerospace research engineer, V/STOL & noise division.

$$\frac{\partial^2 P}{\partial x^2} + \frac{\partial^2 P}{\partial y^2} + (2\pi\eta)^2 P = 0 \qquad (1)$$

where the dimensionless frequency η is given as

$$\eta = \frac{Hf}{c} = \frac{H}{\lambda} \qquad (2)$$

These and all other symbols used in the report are defined in the List of Symbols.

For a hard wall duct infinite in extent, the one-dimensional solution of Eq. (1) for pressure yields[1]

$$P = p^{(1)} + ip^{(2)} = \cos(2\pi\eta x) - i \sin(2\pi\eta x) \qquad (3)$$

The analytical and finite difference solutions for the acoustic pressure of an example case are presented in Fig. 2. To accurately describe the spatial pressure profiles in Fig. 2, the required number of grid points in the x-direction is

$$n = 12\ \eta\left(\frac{L}{H}\right) \qquad (4)$$

For the example shown in Fig. 2, the dimensionless frequency η equals 1 and (L/H) is 1; thus, 12 points are necessary.

Next, consider the example case of a two-dimensional soft-wall duct with $\eta = 1$ and $L/H = 3$. A typical $P^{(1)}$ pressure profile in the suppressor duct is shown in Fig. 3 by the heavy solid line, while the dashed line represents the envelope of the pressure wave amplitude. From Eq. (4), the number of grid points n should be 36. However, if the Helmholtz Eq. (1) could be transformed so that it would describe the envelope (dashed line) of the pressure, the grid points could be reduced to 5 or less, for this particular case as shown in Fig. 3. Since the total number of grid points used is the product of the points in the y-direction with n points in the x-direction, as shown in Fig. 1, this represents a tremendous savings in computer storage and operating time. The task of transforming the Helmholtz equation to the wave envelope equation is now considered.

Generalized Wave Envelope Concept

To remove some (if not all) of the axially oscillatory part of the wave pressure profile, assume

$$P(x,y) = p(x,y)\ e^{-i2\pi\eta^+ x} \qquad (5)$$

where P represents the pressure of the oscillating curve in Fig. 3 and p represents the pressure of the wave envelope shown by the dotted line in Fig. 3, and where

$$\eta^+ = \frac{H}{\lambda^+} \qquad (6)$$

with λ^+ representing the effective axial wavelength of the pressure in the duct (Fig. 3). Substituting Eq. (5) into the Helmholtz equation (1) yields a new governing differenital equation called the Generalized Wave Envelope Equation

$$\frac{\partial^2 p}{\partial x^2} + \frac{\partial^2 p}{\partial y^2} - i4\pi\eta^+ \frac{\partial p}{\partial x} + (2\pi)^2(\eta^2 - \eta^{+2})p = 0 \qquad (7)$$

An example will be presented shortly to illustrate how Eq. (7) can remove the oscillatory nature of the pressure.

For plane waves propagating in hard wall ducts, λ^+ is known to be c/f. For this case Eq. (7) reduces to

$$\frac{\partial^2 p}{\partial x^2} + \frac{\partial^2 p}{\partial y^2} - i4\pi\eta \frac{\partial p}{\partial x} = 0 \qquad (8)$$

In soft wall ducts, λ^+ is not known precisely; therefore, the problem of picking λ^+ (or η^+) to remove the pressure oscillations must be considered. In Ref. 5, λ^+_{soft} was assumed equal to λ^+_{hard}. Later in this section, we will show how the assumption works.

For convenience, the hard wall case, for which the correct answer is known, will now be used to investigate the sensitivity of an incorrect guess on the final answer. To illustrate how Eq. (7) or (8) removes the oscillatory nature of the pressure, consider again the hard wall duct problem of Fig. 2. The exact analytical solution of Eq. (7) for p in which the assumed η^+ term is included is

$$p = p^{(1)} + ip^{(2)} = \cos 2\pi(\eta-\eta^+)x - i\sin 2\pi(\eta-\eta^+)\ x \qquad (9)$$

Of course, the product of Eq. (9) with $e^{-i2\pi\eta^+ x}$ always gives the exact pressure variation P as defined by Eq. (3). That is, every p(x) obtained for any assumed value of η^+ will yield the correct value of P(x) when substituted back into Eq. (3).

The analytical solutions for $p^{(1)}$ from Eq. (9) for various assumed values of η^+ or $|\eta-\eta^+|$ are shown in Fig. 4. For η^+ equals 0, Eq. (7) reduces to the Helmholtz equation, and $P^{(1)} = p^{(1)}$, see dotted line (cosine shape) in Fig. 4. For this particular problem twelve grid points would be required to adequately describe this pressure profile in a difference analysis. However, if η^+ is assumed to have a value of η^+ between 0.7 and 1.3 such that $|\eta-\eta^+|<0.3$, the exact analytical solution for $p^{(1)}$ would require as few as 3 grid points in the difference analysis. The curves for η^+ between 1.0 and 1.3 are mirrow image to those between 0.7 and 1.0 and therefore are not shown. If η^+ is assumed to be equal to η, the curve for $p^{(1)}$ is the straight line, $\eta = 1$ or $|\eta-\eta^+| = 0$. This line represents the envelope of the pressure oscillation. If, for example, it is assumed that $\eta^+ = .8$, the exact solution in Fig. 4 does not represent the true envelope of the pressure oscillation; it is still a gently varying function that requires only a few finite difference grid points to accurately describe its shape. Thus, it is only necessary to pick a value of λ^+ (or η^+) in the vicinity of the true value of λ^+ to get tremendous saving in the grid points required for a finite difference analysis. In so doing the differential Helmholtz equation is transformed to a new form, Eq. (7), which requires fewer grid points in its solution.

As another example, to show how to pick λ^+, consider the problem of predicting the attenuation in a soft wall duct, where η^+ is an unknown. Calculations for the attenuation were made in Ref. 5 using the assumption that η^+ equals η. Fig-

ure 5 from Ref. 5 shows a comparison of the analytical and wave envelope calculation for the optimum soft-wall duct attenuation for various η and L/H values.

Excellent agreement between the analytical and numerical calculations were obtained for the two-dimensional duct example in Ref. 5. For the $\eta = 5$ and $L/H = 6$ case in Fig. 5, the conventional finite difference theory required 3600 grid points while the wave envelope difference theory required only 100 grid points. Thus, a savings of 3500 grid points over the conventional difference theory is obtained. At lower η and L/H, the savings was smaller. For this type of calculation for any assumed value of η^+, it is necessary to check for a converged answer by increasing the number of grid points (m,n) in both x and y direction, as was done in Ref. 5.

Boundary Conditions

In the transverse direction, the acoustic impedance at the wall as shown in Fig. 1 is defined as the ratio of pressure to the transverse velocity. In dimensionless form the impedance ratio can be expressed as[5]

$$\zeta = \frac{Z}{\rho c} = -i2\pi\eta \frac{P}{(\partial P/\partial y)} \tag{10}$$

Substituting the expression for the transformed pressure, Eq. (5), into Eq. (10) yields

$$\frac{\partial p}{\partial y} = \frac{-ia\pi\eta p}{\zeta} \tag{11}$$

which is the same form as Eq. (10) since the η^+ parameter does not enter into the impedance condition.

The exit condition to be presented now allows the numerical solution to be compared to the analytical results for wave propagation in an infinitely long duct. The entrance region of length L in an infinitely long duct with uniform impedance will not have reflections at any position in the duct. The wave propagation in the entrance region of the infinite duct can be represented with a finite length of duct L by choosing the exit impedance at L so that no reflections occur. Consequently, if the exit condition in the numerical analysis is chosen to eliminate reflections at the exit of the duct, the numerical and analytical results should be in close agreement. The exit condition developed in Ref. 5 to meet this condition was shown to be

$$\frac{\partial P}{\partial x} = -i2\pi\eta P \tag{12}$$

Substituting the expression for the transformed pressure, Eq. (5), into Eq. (12) yields

$$\frac{\partial p}{\partial x} = -i2\pi(\eta-\eta^+)p \tag{13}$$

For the entrance pressure profile, the transformed pressure is assumed to be

$$p(1) = 1 \tag{14}$$

$$p(2) = 0 \tag{15}$$

Axial Acoustic Power

The sound power which leaves a duct and reaches the far field is related to the axial intensity. As was shown in Ref. 5, the axial intensity can be expressed in terms of the transformed pressure as

$$I = \frac{\eta^+}{\eta}\left[p(1)2 + p(2)2\right] + \frac{1}{2\pi\eta}\left[p(2)\left(\frac{\partial p(1)}{\partial x}\right) - p(1)\left(\frac{\partial p(2)}{\partial x}\right)\right] \tag{16}$$

It should be noted that the calculated value of intensity will be independent of the assumed value of η^+. The total dimensionless acoustic power is the integral of the intensity across the test section

$$E_x = \int_0^1 I(x,y)dy \tag{17}$$

By definition the decrease, in decibels, of the acoustic power from 0 to x can be written as

$$\Delta dB = 10 \log_{10}\left(\frac{Ex}{E_0}\right) \tag{18}$$

Difference Equations

The continuous system is now reduced to an equivalent lumped-parameter system by means of a finite difference approximation. Instead of a continuous solution for the pressure, the pressure is determined at the isolated grid points shown in Fig. 1. The difference equations to follow are generated using Green's Theorem.

Central

The generalized wave envelope Eq. (7) written in finite difference form for the i,j point in Fig. 1 is

$$\left(\frac{\Delta x}{\Delta y}\right)^2 P_{i,j-1} + \left[1 + i2\pi\Delta x\eta^+\right] P_{i-1,j} - 2\left[1 + \left(\frac{\Delta x}{\Delta y}\right)^2 - \frac{(2\pi\Delta x)^2(\eta^2 - \eta^{+2})}{2}\right] P_{i,j} + \left[1 - i2\pi\Delta x\eta^+\right] P_{i+1,j} + \left(\frac{\Delta x}{\Delta y}\right)^2 P_{i,j+1} = 0 \tag{19}$$

Wall

The difference equation which applies along the upper boundary in Fig. 1 is

$$\left(\frac{\Delta x}{\Delta y}\right)^2 P_{i,m-1} + \frac{1}{2}\left[1 + i2\pi\Delta x\eta^+\right] P_{i-1,m} - \left[1 + \left(\frac{\Delta x}{\Delta y}\right)^2 - \frac{(2\pi\Delta x)^2(\eta^2 - \eta^{+2})}{2} + \frac{i2\pi\eta\Delta x^2}{\zeta\,\Delta y}\right] P_{i,m} + \frac{1}{2}\left[1 - i2\pi\Delta x\eta^+\right] P_{i+1,m} = 0 \tag{20}$$

A similar equation applies along the lower wall.

Exit

The difference equation which applies along the exit plane in Fig. 1 is

$$\frac{1}{2}\left(\frac{\Delta x}{\Delta y}\right)^2 p_{n,j-1} + \left[1 + i2\pi\Delta x\eta^+\right] p_{n-1,j} - \left[1 + \left(\frac{\Delta x}{\Delta y}\right)^2 - \frac{(2\pi\Delta x)^2(\eta^2 - \eta^{+2})}{2} + i2\pi\Delta x(\eta - \eta^+) + i2\pi\Delta x\eta^+\right] p_{n,j} + \frac{1}{2}\left(\frac{\Delta x}{\Delta y}\right)^2 p_{n,j+1} = 0 \qquad (21)$$

Corner

The difference equation which applies at the upper corner (point n,m in Fig. 1) is given by

$$\frac{1}{2}\left(\frac{\Delta x}{\Delta y}\right)^2 p_{n,m-1} + \frac{1}{2}\left[1 + i2\pi\Delta x\eta^+\right] p_{n-1,m} - \frac{1}{2}\left[1 + \left(\frac{\Delta x}{\Delta y}\right)^2 - \frac{(2\pi\Delta x)^2(\eta^2 - \eta^{+2})}{2} + \frac{i2\pi\eta\Delta x^2}{\zeta\,\Delta y} + i2\pi\Delta x\,(\eta - \eta^+) + i2\pi\Delta x\eta^+\right] p_{n,m} = 0 \qquad (22)$$

a similar equation exist for the lower corner.

Axial Intensity

In terms of the difference notation, the axial intensity as given by Eq. (16) can be expressed as

$$I = \frac{\eta^+}{\eta}\left[p_{i,j}^{(1)2} + p_{i,j}^{(2)2}\right] + \frac{1}{2\pi\eta}\left[p_{i,j}^{(2)}\left.\frac{\partial p^{(1)}}{\partial x}\right|_{i,j} - p^{(1)}\left.\frac{\partial p^{(2)}}{\partial x}\right|_{i,j}\right] \qquad (23)$$

The total power across a particular cross section, as given by Eq. (17), is written in difference notation as

$$E_i = \left[\frac{1}{2} I_{i,1} + \sum_{j=2}^{m-1} I_{i,j} + \frac{1}{2} I_{i,m}\right]\Delta y \qquad (24)$$

By evaluating E_i at the entrance and exit positions, taking the log of their ratio and multiplying by 10, as indicated in Eq. (18), the sound attenuation for the duct is determined.

Matrix Solutions

The collection of the various difference equations at each grid point forms a set of simultaneous equations which can be expressed in matrix notation as

$$\{\overline{A}\}\,[\overline{p}] = [\overline{F}] \qquad (25)$$

where $\{A\}$ is the known coefficient matrix, $[\overline{p}]$ is the unknown pressure vector, and $[\overline{F}]$ is the known column vector containing the various initial conditions. The matrix is complex. At the present time, the most efficient computer routine for solving Eq. (25) was written by D. W. Quinn[4] at Wright-Patterson Air Force Base, Dayton, Ohio. Equation (25) can also be solved by subdividing the complex matrix into four real matrices. The real matrices can be solved using standard elimination techniques.

Results and Discussion

Calculations are now presented in this section to illustrate the use of the wave envelope concept in solving two sample problems in treated duct attenuation: the effect of source strength radial profile; and the effect of variable axial impedance. In the following calcualtions η^+ will be assumed to η. In all calculations, the fact that the pressure profile are symmetric about the centerline was used to reduce the required number of grid points in y-direction.

Radial Source Profiles

Because of the complexities of the turbo-fan noise source, questions exist at the present time on the radial distribution of the acoustic energy at the fan source. The attenuation was therefore calculated for stepped noise source profiles of the form illustrated in Fig. 6. The calculation were made for a liner which had been optimized assuming a uniform source profile. The sensitivity of the liner attenuation for various size of the steps was determined at three different frequencies.

Figure 7(a), (b), and (c) illustrates the results for the three cases of $\eta = 1$, 2, and 5, and all at $L/H = 1$. In each of these figures, the abscissa represents the radial position of the step in the duct. The attenuation for a duct with a uniform radial profile is represented by the far left ahnd portion of the curve at $y = 0$. As the radial position of the step moves to the right towards the absorbing wall, $y > 0$, a greater portion of the energy will be absorbed. As seen in Fig. 7(a), for a low frequency source ($\eta = 1$) a modest (3 dB) increase in attenuation is seen for either profile as compared with the attenuation of the uniform profile. However, as shown in Figs. 7(b) and 7(c), for the smaller wavelength sound sources ($\eta = 2$ and 5) the attenuation for the stepped profiles is much larger than for the uniform profiles.

Higher order modes have been shown by analysis, in general, to have higher damping coefficients than the lower order modes. Since such a step pressure profile can be considered to be composed of various higher-order radial modes, and since higher-order modes (stepped towards wall) damp more quickly than the lower-order modes, the results seen here are in qualitative agreement with analytical theories[6].

In a practical problem, if the noise source profile of a turbo-fan engine is skewed with a higher concentration of acoustic intensity closer

to the wall, the attenuation predicted assuming a uniform source would under-perdict the measured attenuation.

Wall Impedance Variation

To eliminate the need for heavy, expensive and otherwise undesirable splitter rings and also to reduce the required length of wall treatment (cowl length), recent research is concerned with increasing the attenuation of wall treatment in a fixed length of liner. One practical approach to increasing the attenuation of a liner[7] is to subdivide the liner into several different segments as shown in Fig. 8. Next, to obtain higher attenuations than are possible with a uniform liner, the liner segments are jointly optimized to maximize the noise attenuation.

In optimizing the stepped liners, the starting point was the optimized uniform impedance. The first liner segment was then optimized while holding the remaining segments at the uniform value. Next, holding the first segment at its new value, the iteration process was continued on the remaining segments. The process was repeated for the whole liner until the change in the duct attenuation was less than 5%.

Figure 9 shows the optimum attenuation determined herein for stepped impedances of two and three steps for a dimensionless frequency of $\eta = 1$ and a liner length-to-height ratio L/H of 0.5. As seen in Fig. 9, the two and three stepped liners have increased the attenuation by 5 and 6 dB respectively. Figure 10 shows the optimum attenuation for a two step duct at the higher dimension less frequency of $\eta = 5$. These calculations for $\eta = 1$ and $\eta = 5$ show that the stepped impedance ducts have theoretical attenuation 2.0 to 2.5 times the attenuation of a uniform impedance liner of the same length. The dotted part of the curve shown in Fig. 10 is an numerical instability that results from insufficient grid points. As shown in Ref. 5, the number of grid points in y-direction should be increased for increasing η. Unfortunately, the present computer program could not accomidate the required increase in grid points.

In both the two and three-stepped liners for $\eta = 1$ and a two stepped liner for $\eta = 5$, the resistive component of impedance optimized near zero (0.01) in the first segment of the liner. As a result, the first portion of the segmented liner removes less acoustic energy than the uniform liner. This can be seen in Fig. 9 by observing that the curves for both the two and three-step liners fall below the curve for the uniform liner for x less than 0.3. This is to be expected since there is no resistive component of impedance to dissipate the energy in the first segment of the stepped liners.

The reactive component of the first section of the two and three stepped liners does not differ substantially from the optimum reactance for a uniform liner with a plane wave input, or from the optimum reactance associated with the least attenuated mode in a uniform duct.

The reasons for the enhanced attenuation for the stepped duct liner over the uniform liner can be reduced from the work in Ref. 4 concerning the acoustic boundary layer and the results presented earlier on stepped noise source profiles. In uniform impedance liners, an "acoustic pressure diffusion boundary layer" is formed along the walls. The acoustic pressure at the centerline of the duct is "unaware" of the soft wall until the acoustic diffusion boundary layer at the upper and lower walls meet. This is illustrated by the results shown in Fig. 11. This phenomenon is analogous to the problem of a developing laminar velocity profile in the entrance region of a pipe. It takes a prescribed length down the pipe before the growing laminar boundary layers at the walls meet in the center of the pipe to establish the fully developed parabolic laminar flow profile. Apparently the low resistive entrance impedance induces large transverse movement of the acoustic energy which break up the "acoustic diffusion boundary layer" and redistributes the acoustic energy towards the wall in the entrance section of the duct. The redistribution of acoustic energy towards the wall is illustrated for the two-stepped liner in Fig. 12, which compares the sound pressure level (SPL) for the two-stepped and the uniform impedance liners. As seen in Fig. 12, the SPL in the initial segment of the duct increases in the vicinity of the wall. As was shown in the earlier section of this report on radial distribution effects of sound sources, if the acoustic pressure profile is peaked nearer to the wall, the acoustic energy in the duct can be more effectively absorbed. This phenomenia could be called pressure redistribution. The pressure source is conditioned for better absorption by the downstream liner segments. As seen in Fig. 12, the peak SPL level which occurred at $x = 0.25$ is quickly lowered below the uniform SPL level at the point $x = 0.375$.

To fabricate a low-resistive element, large open area in the acoustic liner is required. For the no flow case considered here, a closely packed array of quarter-wave tubes might be ideal in this application since these tubes can be tuned to give the proper reactance yet still have a very low resistance. However, a practical liner may have a higher resistance than the desired optimum value. In this case, the efficiency of the liner would be reduced. The sensitivity of the liner attenuation to the entrance resistance is shown in Fig. 13. As seen in Fig. 13, the efficiency of the liner decreases with increasing resistance of the first segment. Consequently, both theoretical and experimental work is needed on the design of low-resistance liners.

Combined Stepped Segments and Source Profile

Finally, suppose a stepped noise source profile of the form shown in Fig. 6 exits in the duct. Such a profile might result because more noise is generated at the tip of the rotor or because a centerbody channels more acoustic energy to the vicinity of the wall. Suppose we also want to use a two-stepped segmented liner. For a stepped profile which extends 30% inward from the wall, the optimum impedance was determined for a two stepped duct. The results shown in Fig. 14, are compared with the uniform impedance optimized for both a step input and a plane wave input. In this example, the resistance of the initial segment is at 0.11. This is higher than the resistance required for the plane wave source input for a two-stepped liner. Recall that the resistance for the two-step liner for a uniform plane wave input was shown to be

0.01 in Fig. 9. Most likely, since the acoustic pressure is already higher in the vicinity of the wall, the optimum resistance in the first section of the stepped duct is higher so that acoustic energy can be immediately absorbed. Clearly, the optimum impedance distribution will be a function of the source noise distribution.

Recall that for a uniform duct with a plane wave input, for $\eta = 1$ and $L/H = 0.5$ the attenuation is -4 dB, as shown in Fig. 9. Comparing this value to the nearly -40 dB attenuation shown in Fig. 14 for a stepped noise source profile and a segmented liner, the combined consideration of both source profiles and segmented liners can be a significant in the design of an acoustic liner.

Conclusions

Because the wave envelope technique greatly reduces the required computer storage and solution time, the technique was conveniently applied to the acoustic problems of skewed inlet pressure waves and ducts with axial variations in impedance. For both plane wave uniform noise sources and stepped noise sources, segmented liners are shown theoretically to increase the attenuation as compared to a uniform liner by redistributing the energy to the wall so that the acoustic energy can be more efficiently absorbed by the liner. To accomplish this redistribution of energy, the first element of the segmented liner must have a value of resistance near zero. For higher initial segment resistance, the attenuation significantly falls below the optimum value. The optimization of segmented impedance components and the optimum attenuation of the liner are shown to be strong functions of the source noise distribution.

References

1. Baumeister, K. J. and Bittner, E. C., "Numerical Simulation of Noise Propagation in Jet Engine Ducts," TN D-7339, Oct. 1973, NASA.

2. Baumeister, K. J. and Rice, E. J., "A Difference Theory for Noise Propagation in Acoustically Lined Duct with Mean Flow," AIAA Paper 73-1006, Seattle, Wash., 1973.

3. Alfredson, R. J., "A Note on the Use of the Finite Difference Method for Predicting Steady State Sound Fields," Acustica, Vol. 28, No. 5, 1973, pp. 296-301.

4. Quinn, D. W., "A Finite Difference Method for Computing Sound Propagation in Non-Uniform Ducts," AIAA Paper 75-130, Pasadina, Calif., 1975.

5. Baumeister, K. J., "Analysis of Sound Propagation in Ducts Using the Wave Envelope Concept, Concept," TN D-7719, July 1974, NASA.

6. Rice, E. J., "Spinning Mode Sound Propagation in Ducts with Acoustic Treatment," presented at 88th Acoustical Society of America meeting, St. Louis, Mo., Nov. 1974; also NASA TM X-71613, 1974.

7. Lansing, D. L. and Zorumski, W. E., "Effects of Wall Admittance Changes on Duct Transmission and Radiation of Sound," Journal of Sound Vibration, Vol. 27, No. 1, Mar. 1973, pp. 85-100.

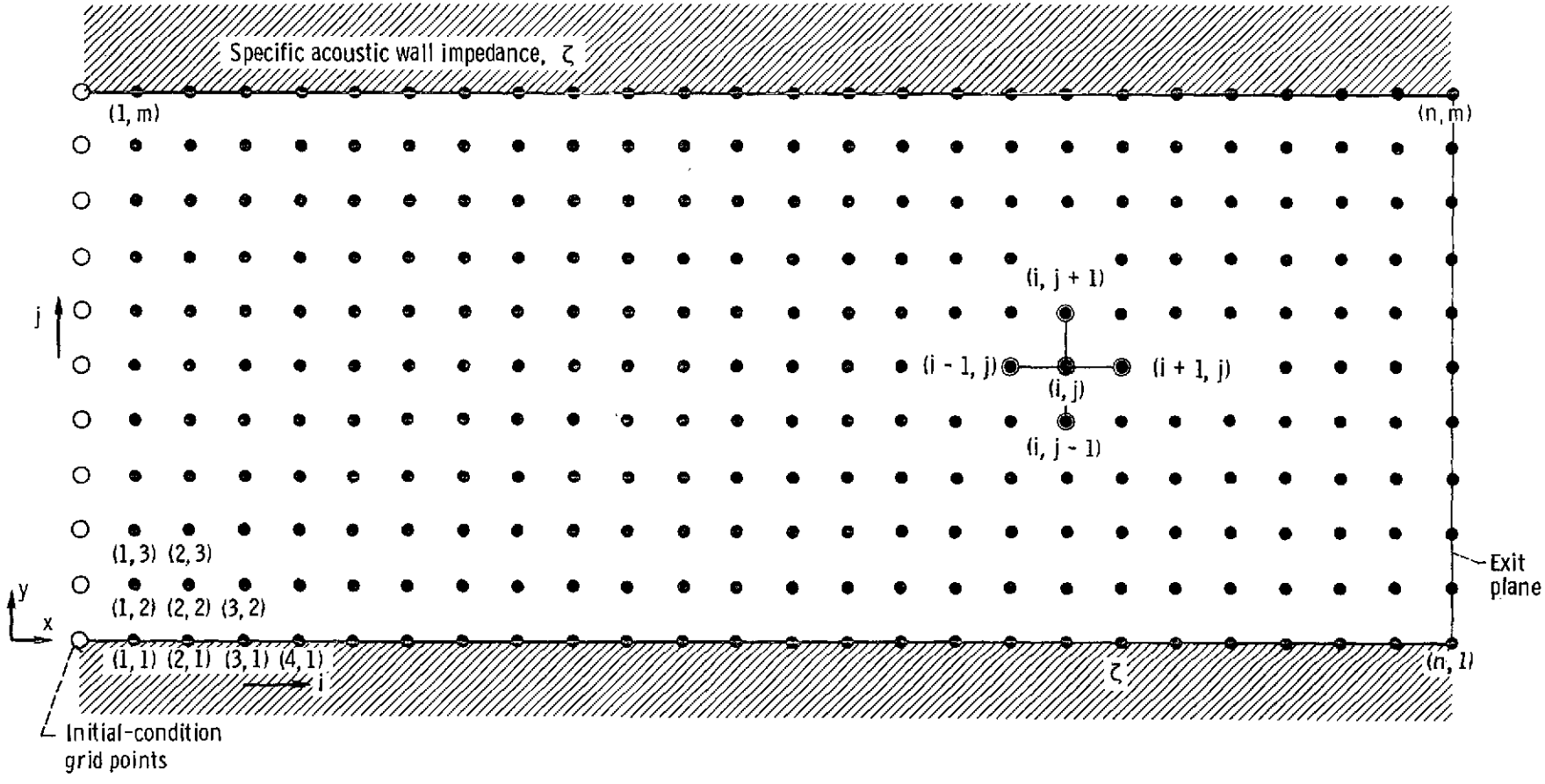

Figure 1. - Grid-point representation of two-dimensional flow duct.

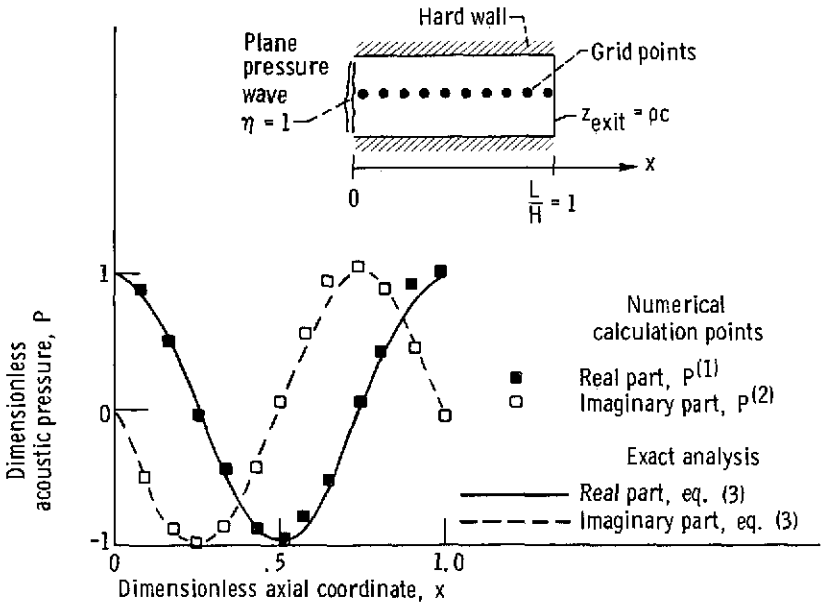

Figure 2. - Analytical and numerical pressure profiles for one-dimensional sound propagation in hard-wall duct. Dimensionless frequency $\eta = 1$. $P = P^{(1)} + iP^{(2)}$.

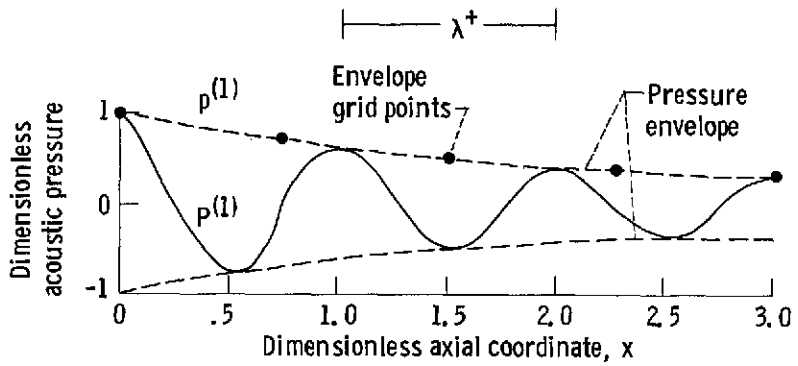

Figure 3. - Typical pressure profile for sound propagation in a two dimensional soft-wall duct for dimensionless frequency $\eta = 1$ and duct length $L/H = 3$.

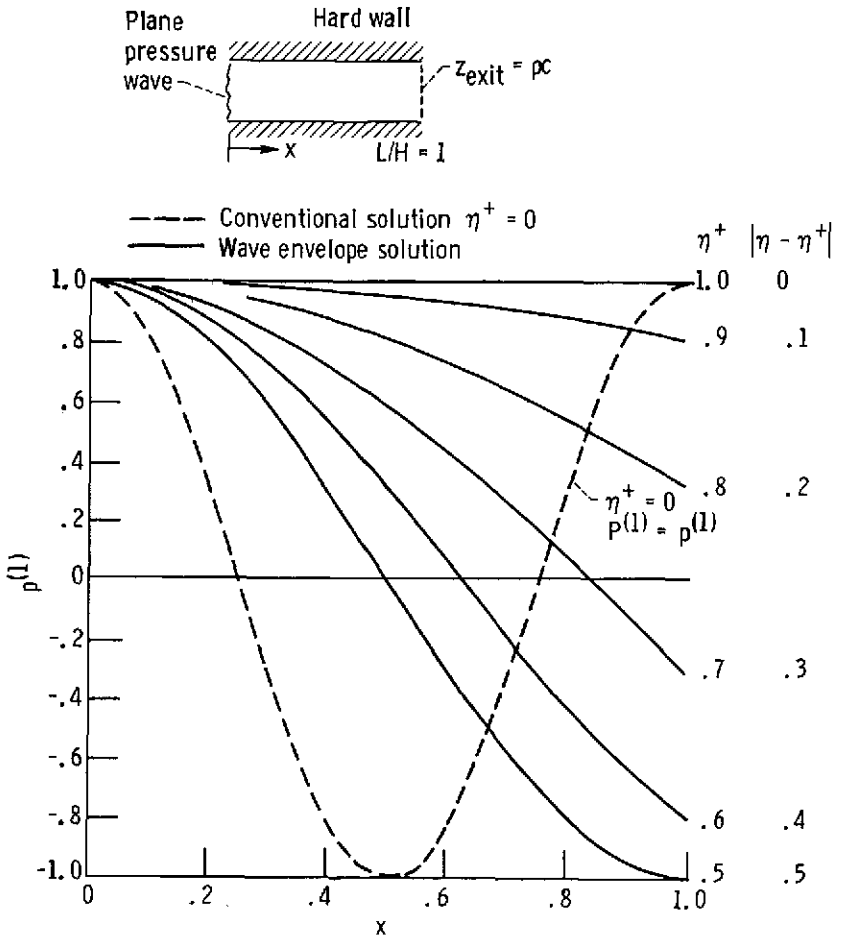

Figure 4. - Sensitivity of the real pressure component $p^{(1)}$ to the choice of η^+ for a hard wall duct with $\eta = 1$ and L/H = 1.

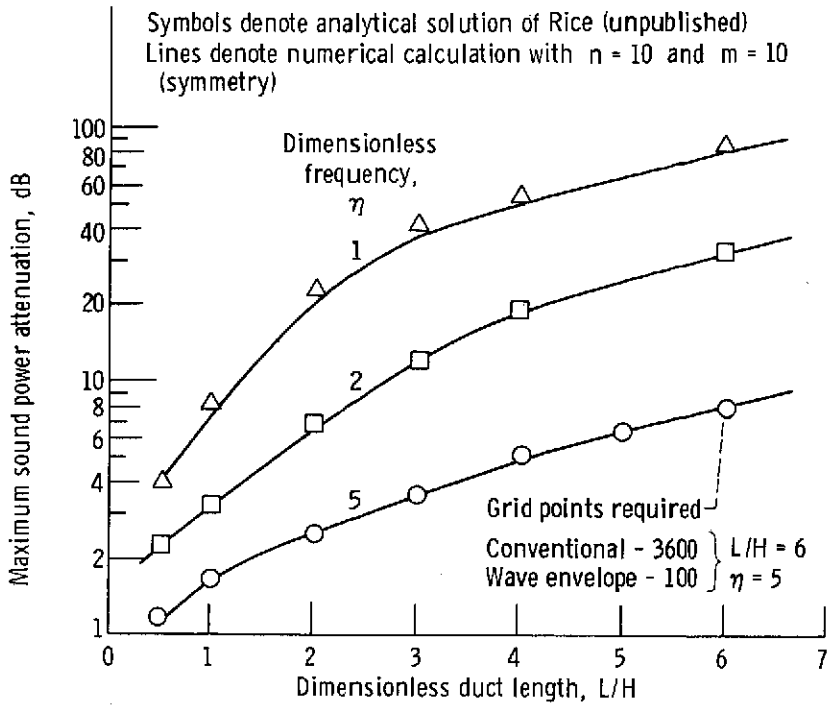

Figure 5. - Effect of axial length and frequency on attenuation at optimum impedance in two-dimensional duct assuming $\eta^{+} = \eta$ (ref. 5).

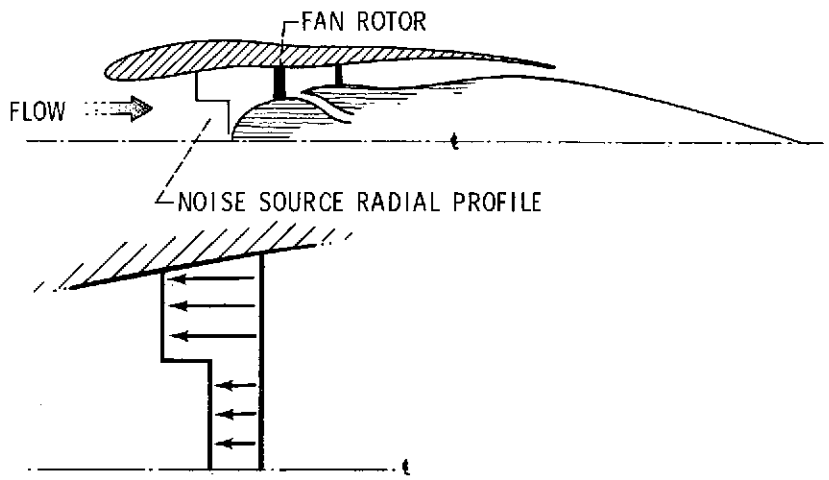

Figure 6. - Illustration of noise source profile in inlet of turbo-fan engine.

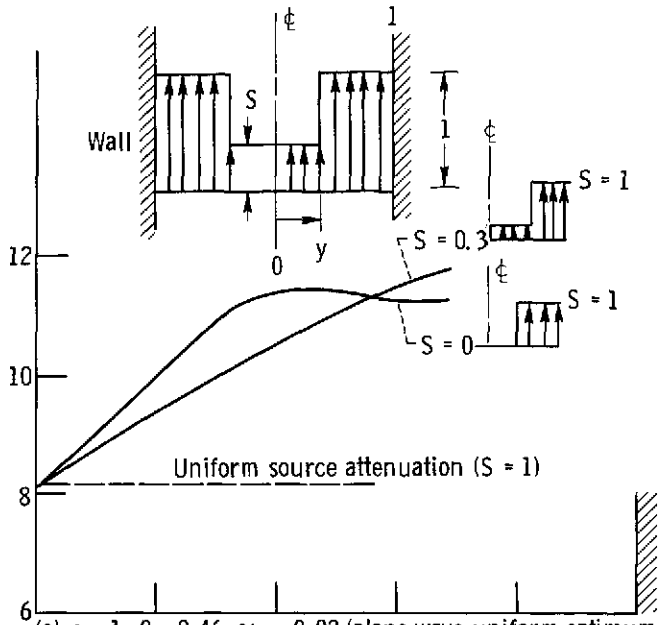

(a) $\eta = 1$, $\theta = 0.46$, $\chi = -0.92$ (plane wave uniform optimum impedance).

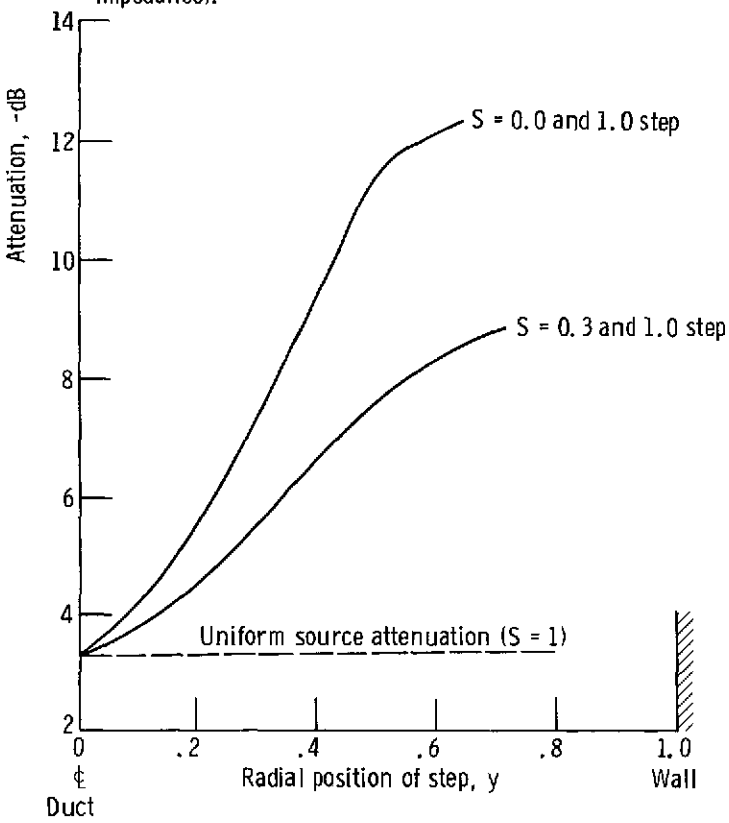

(b) $\eta = 2$, $\theta = 0.47$, $\chi = -1.32$ (plane wave optimum impedance).

Figure 7. - Effect of transverse stepped source profiles on duct attenuation for L/H = 1 and zero and 0.3 step for m = 14, n = 10 at the η and impedance values indicated in each figure.

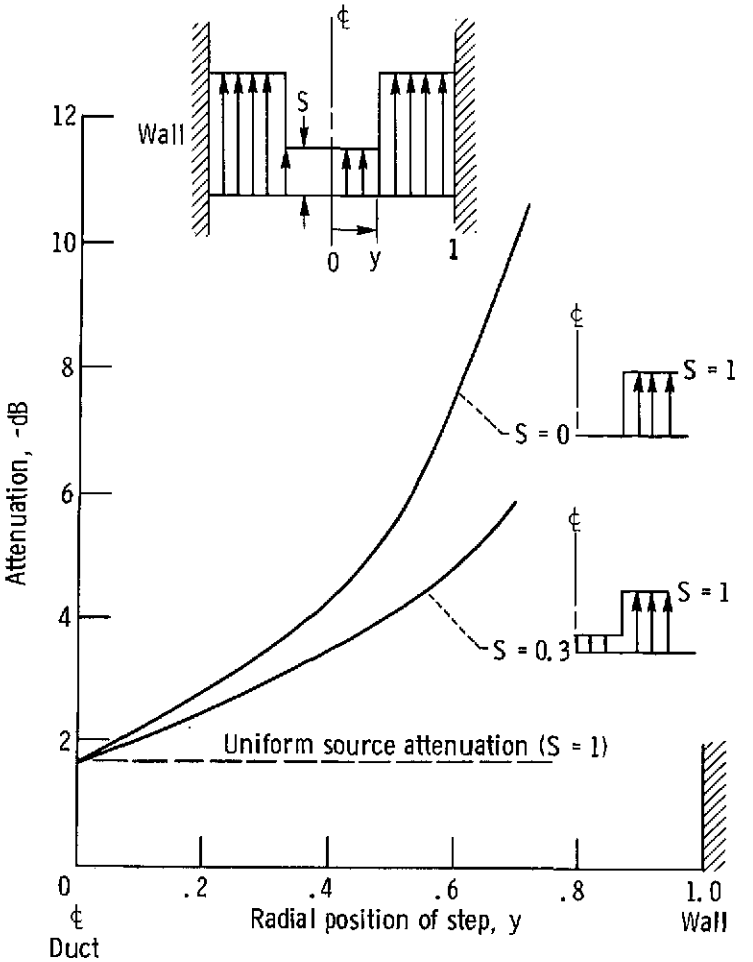

(c) $\eta = 5$, $\theta = 0.84$, $\chi = -2.2$ (plane wave optimum impedance).

Figure 7. - Concluded.

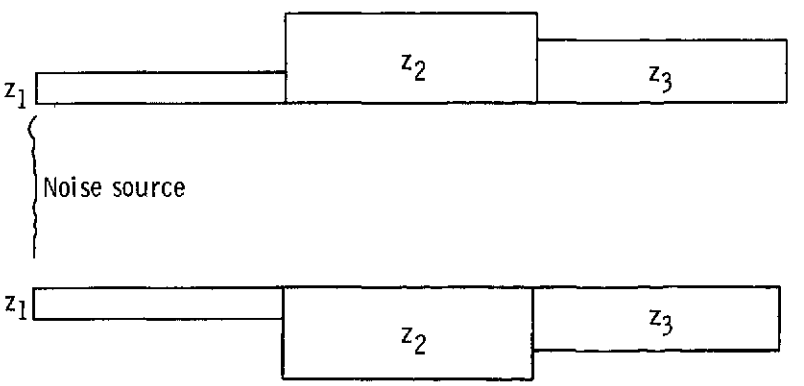

Figure 8. - Stepped duct liner with segments of varied impedance.

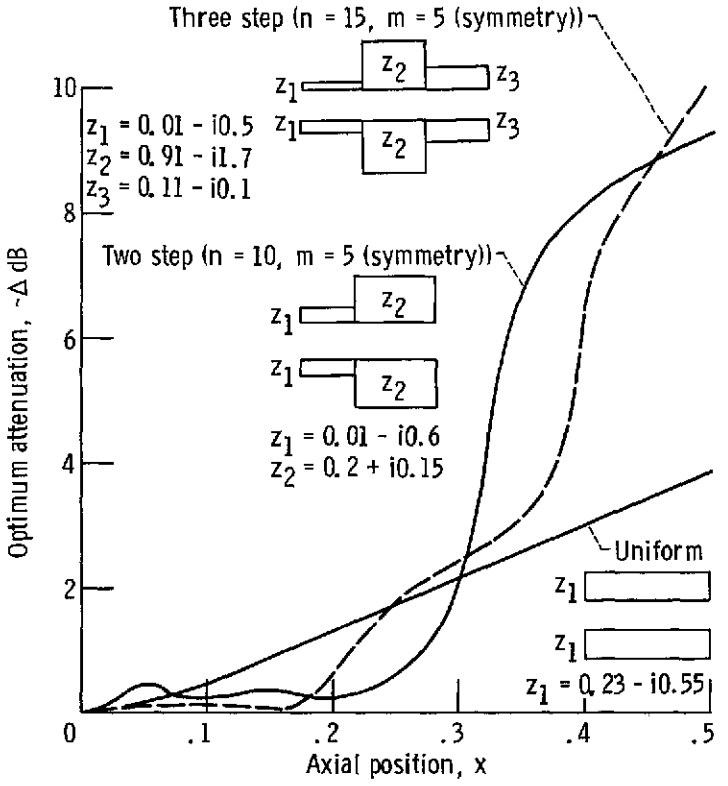

Figure 9. - Impedance optimized for an L/H = 0.5 and η = 1.

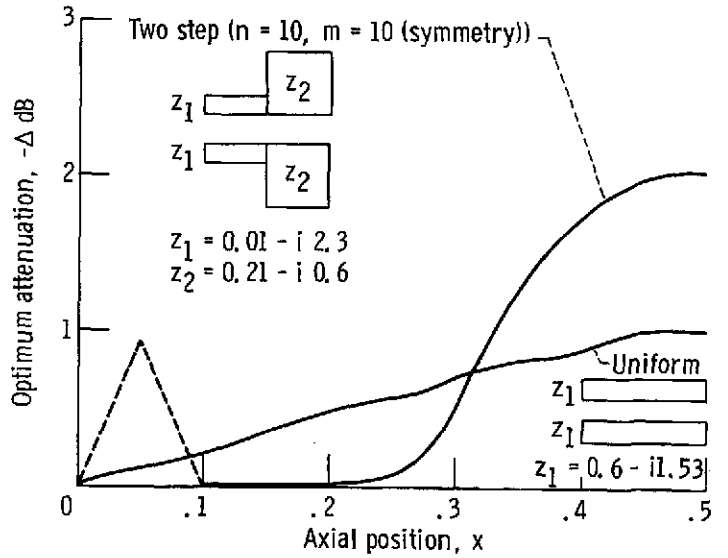

Figure 10. - Impedances optimized for an L/H = 0.5 and η = 5.

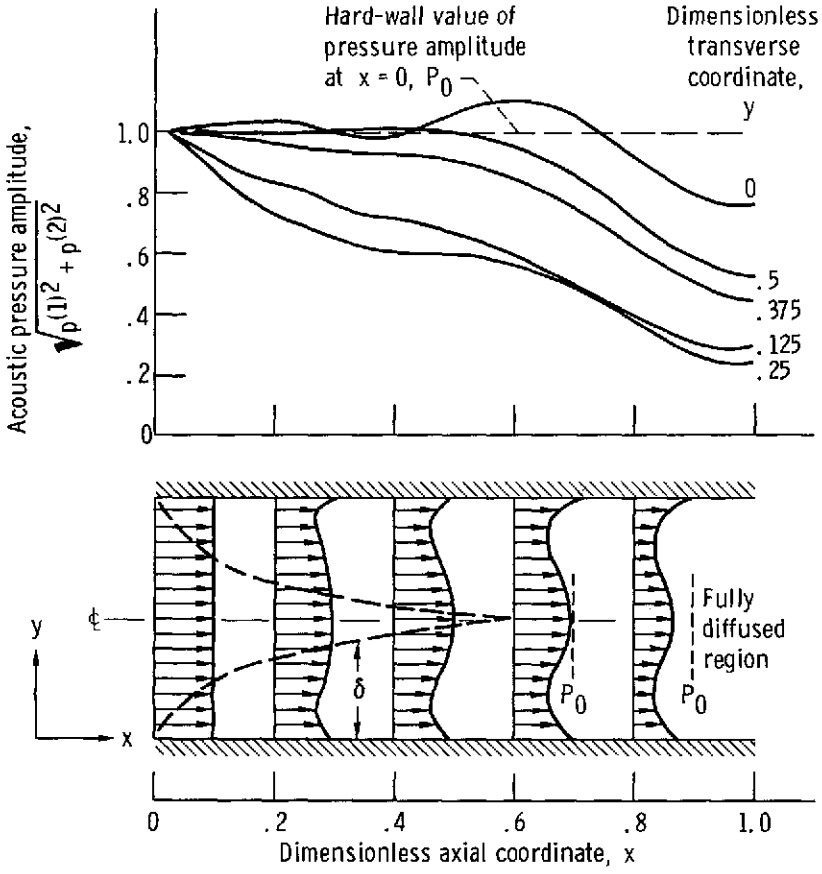

Figure 11. - Pressure amplitude fluctuations along duct at optimum impedance for dimensionless frequency $\eta = 1$, dimensionless duct length $L/H = 1$, number of grid rows $m = 10$, and number of grid columns $n = 10$ (ref. 5).

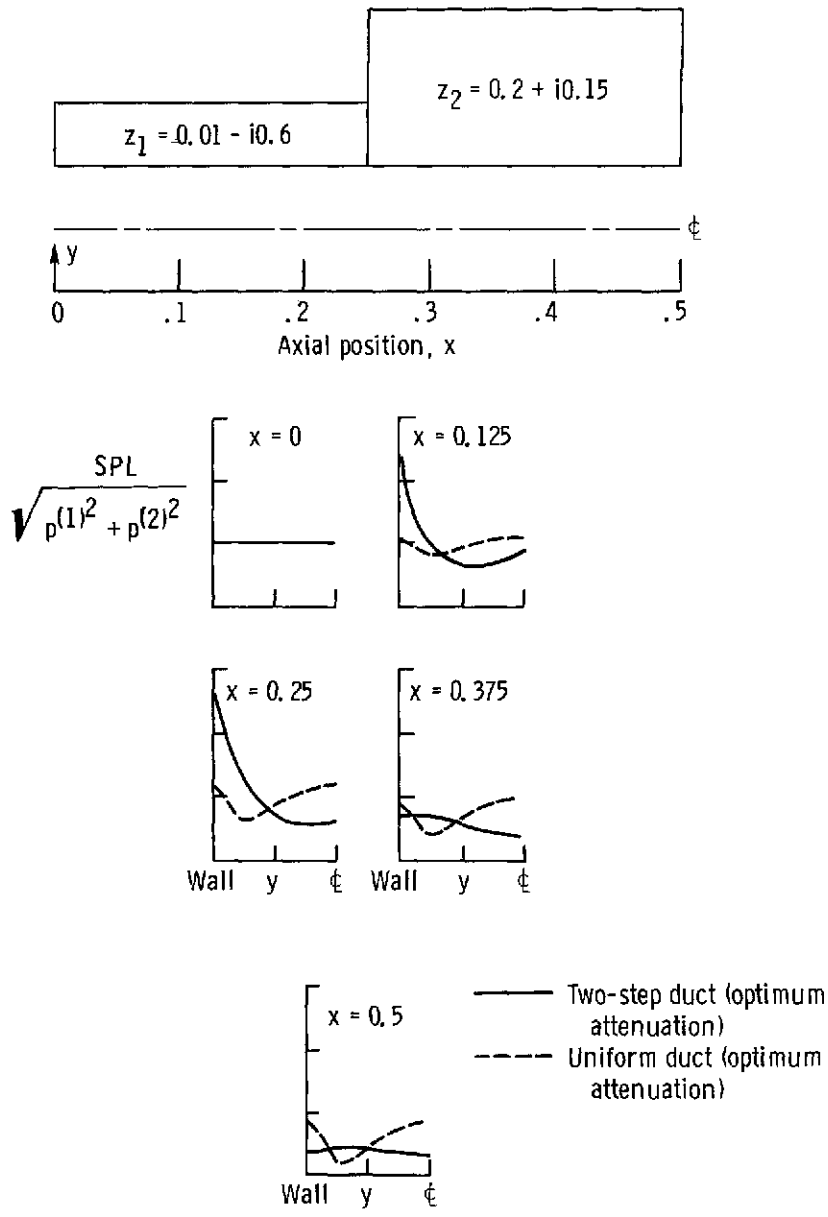

Figure 12. - Radial SPL profiles for uniform and two-step duct liners for $\eta = 1$ and $L/H = 0.5$ for $m = 5$, $n = 10$.

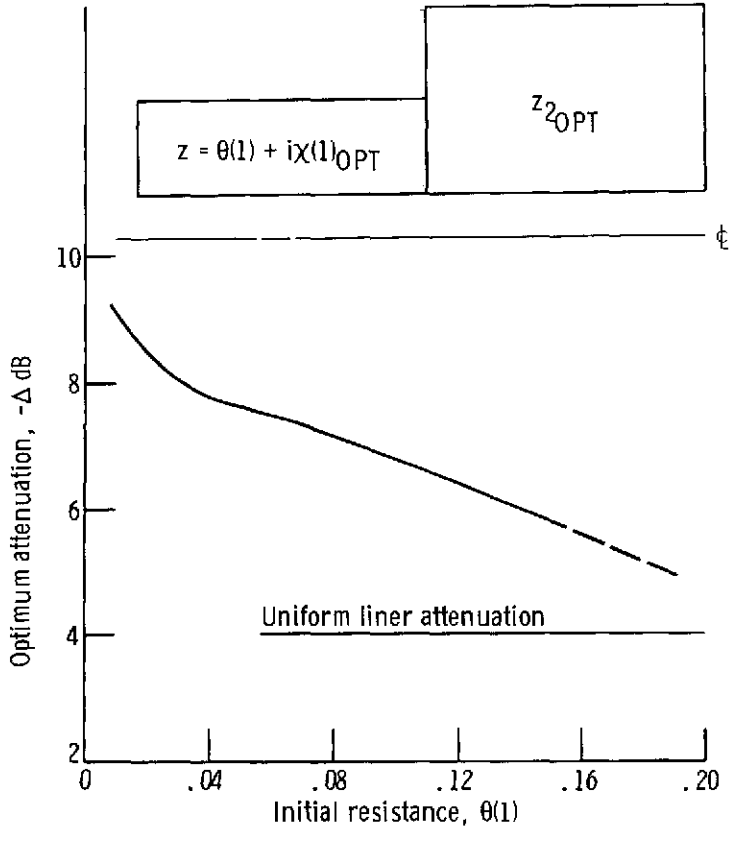

Figure 13. - Effect of initial stepped specific acoustic resistance θ(1) on maximum attenuation in a two-step duct for $\eta = 1$, L/H = 0.5, m = 5 (symmetry), n = 10.

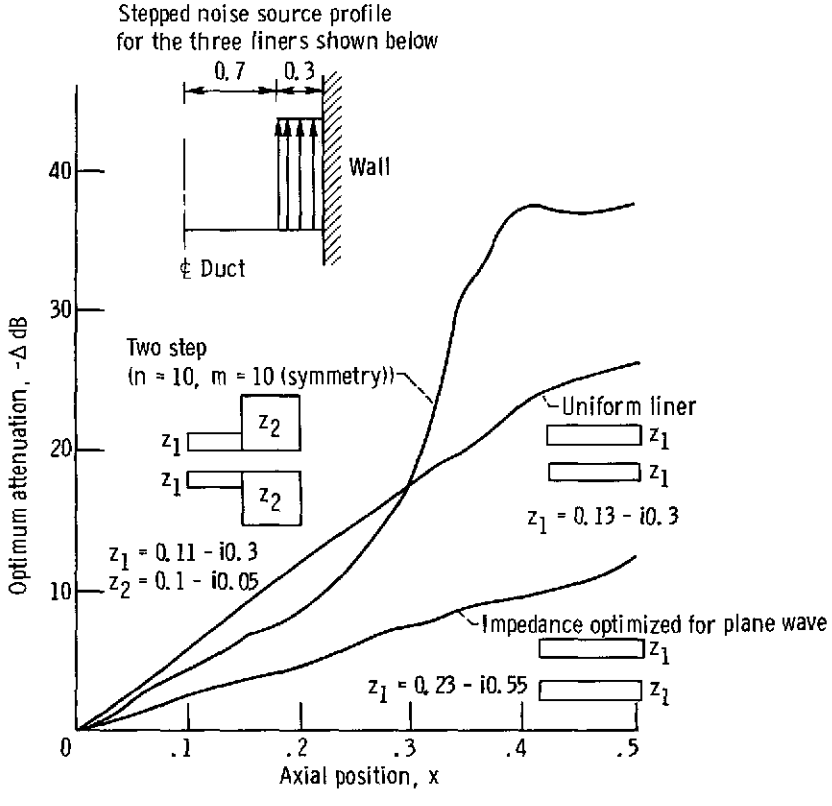

Figure 14. - Impedances optimized for a stepped noise source profile and two segment liner for $\eta = 1$ and L/H = 0.5.

NASA-Lewis